Imaging Imidazoline-I_2 Binding Sites in Porcine Brain Using ^{11}C-BU99008

Steven Kealey[1,2], Emma M. Turner[3], Stephen M. Husbands[3], Cristian A. Salinas[2], Steen Jakobsen[4], Robin J. Tyacke[5], David J. Nutt[5], Christine A. Parker[2,5], and Antony D. Gee[6]

[1]Institute of Psychiatry, De Crespigny Park, King's College London, London, United Kingdom; [2]Imanova Ltd., Hammersmith Hospital, London, United Kingdom; [3]Department of Pharmacy and Pharmacology, University of Bath, Bath, United Kingdom; [4]PET Center, Aarhus University Hospital, Aarhus, Denmark; [5]Neuropsychopharmacology Unit, Hammersmith Hospital, Imperial College London, London, United Kingdom; and [6]Division of Imaging Sciences and Biomechanical Engineering, King's College London, Rayne Institute, London, United Kingdom

Changes in the density of imidazoline-I_2 binding sites have been observed in a range of neurologic disorders including Alzheimer's disease, Huntington's chorea, and glial tumor; however, the precise function of these sites remains unclear. A PET probe for I_2 binding sites would further our understanding of the target and may find application as a biomarker for early disease diagnosis. Compound BU99008 has previously been identified as a promising I_2 ligand from autoradiography studies, displaying high affinity and good selectivity toward the target. In this study, BU99008 was radiolabeled with ^{11}C in order to image the I_2 binding sites in vivo using PET. **Methods:** ^{11}C-BU99008 was radiolabeled by *N*-alkylation of the desmethyl precursor using ^{11}C-methyl iodide. A series of PET experiments was performed to investigate the binding of ^{11}C-BU99008 in porcine brains, in the presence or absence of a nonradiolabeled, competing I_2 ligand, BU224. **Results:** ^{11}C-BU99008 was obtained in good yield and specific activity. In vivo, ^{11}C-BU99008 displayed good brain penetration and gave a heterogeneous distribution with high uptake in the thalamus and low uptake in the cortex and cerebellum. ^{11}C-BU99008 brain kinetics were well described by the 1-tissue-compartment model, which was used to provide estimates for the total volume of distribution (V_T) across brain regions of interest. Baseline V_T values were ranked in the following order: thalamus $>$ striatum $>$ hippocampus $>$ frontal cortex $\geq$ cerebellum, consistent with the known distribution and concentration of I_2 binding sites. Administration of a selective I_2 binding site ligand, BU224, reduced the V_T to near-homogeneous levels in all brain regions. **Conclusion:** ^{11}C-BU99008 appears to be a suitable PET radioligand for imaging the I_2 binding sites in vivo.

Key Words: PET; imidazoline; I_2; BU99008; ^{11}C

J Nucl Med 2013; 54:139–144
DOI: 10.2967/jnumed.112.108258

Imidazoline binding sites were first identified by Bousquet et al. in 1984, after their observation that the antihypertensive drug, clonidine, interacted with a distinct imidazoline-preferring site in addition to the α_2-adrenoceptor (*1*). Imidazoline binding sites have since been characterized in a variety of species and tissues and divided into 3 separate pharmacologic subtypes, termed the I_1, I_2, and I_3 binding sites (*2*). Although functions have been demonstrated for the I_1 sites (blood pressure regulation) and I_3 sites (modulation of insulin release), the precise role of the I_2 sites is unclear. The physiologic relevance of I_2 binding sites is supported by studies that find the endogenous substances agmatine (*3*) and harmane (*4*) to have significant activity at one or more of these sites. Additionally, I_2 sites have been linked to several central nervous system disorders for which changes in the binding density have been observed in postmortem brain tissue. These include depression (*5,6*), addiction (*7*), glial tumor (*8–10*), and neurodegenerative disorders such as Alzheimer's disease (*11*) and Huntington's chorea (*12*). An in vivo imaging probe to study I_2 sites in living tissue would therefore prove invaluable in further delineating the precise physiologic role of these binding sites in healthy and disease states.

PET is an in vivo imaging technique that uses radioligands as selective molecular probes to map the location and density of specific proteins. The development of a selective I_2 PET radioligand would allow for the characterization of I_2 binding sites in vivo and their regulation in disease states. Although several ligands selective for I_2 sites have been reported (*13*), only 2 potential PET radioligands have been reported to date. Roeda et al. (*14*) published the radiosynthesis of ^{11}C-benazoline in 2003; however, its study in vivo has not been reported. Most recently, Kawamura et al. reported the in vivo imaging of ^{11}C-FTIMD in rats (*15*) and in monkeys (*16*), although the specific signal appears to be low in both cases. In this article, we report the synthesis and initial preclinical in vivo evaluation of ^{11}C-BU99008 as a novel PET radioligand for imaging I_2 binding sites.

Received May 4, 2012; revision accepted Aug. 6, 2012.
For correspondence or reprints contact: Steven Kealey, Institute of Psychiatry, King's College London, Denmark Hill, London, SE5 8AF, U.K.
E-mail: steven.kealey@kcl.ac.uk
Published online Dec. 5, 2012.

MATERIALS AND METHODS

Chemistry

Solvents were of high-performance liquid chromatography (HPLC) grade and were purchased from Aldrich. Labeling reactions were performed using anhydrous Sure/Seal solvents from Aldrich. ^{11}C-CH_4 was produced using an IBA Cyclone 18/18 Twin cyclotron by the $^{14}N(p,\alpha)^{11}C$ nuclear reaction using a nitrogen gas target (containing 5% hydrogen) pressurized to 150 psi and bombarded with 18-MeV protons. Subsequently, ^{11}C-CH_4 was converted into ^{11}C-CH_3I by gas-phase iodination with iodine using a ProC system (GE Healthcare). The labeling procedure was performed using a fully automated system (ProC) including ^{11}C-methylation, HPLC purification, and labeled product formulation. The precursor for radiolabeling, 2-(4,5-dihydro-1H-imidazol-2-yl)-1H-indole (BU99007), was synthesized according to the method described by Tyacke et al. (*17*).

Radiochemical Synthesis of ^{11}C-BU99008

^{11}C-BU99008 was prepared by *N*-alkylation of the precursor BU99007 using ^{11}C-CH_3I (Fig. 1). BU99007 (1.0 mg) was dissolved in dimethylformamide (300 μL) in a 1-mL glass vial, and tetrabutylammonium hydroxide (20 μL of a 0.1 M methanol solution) was added. ^{11}C-CH_3I was delivered to the vial at room temperature in a helium carrier gas stream. After ^{11}C-CH_3I delivery, the vessel was heated at 120°C for 5 min and injected onto the semipreparative HPLC column (Eclipse SB-phenyl column [Agilent]; 250 × 9.4 mm). HPLC purification was performed with a mobile phase of acetonitrile and ammonium formate (50 mM; pH 9.9; 50:50) at a flow rate of 10 mL/min. The product fraction (retention time, ~5.5 min) was collected and diluted with 100 mL of water. This solution was passed through a C_{18} Sep-Pak (Waters), rinsed with water (10 mL), and eluted off with ethanol (1 mL), followed by saline (9 mL). The analysis of chemical and radiochemical purity was performed by analytical HPLC (Eclipse SB-phenyl column; 150 × 4.6 mm) using a mobile phase of acetonitrile and ammonium formate (50 mM; pH 9.9; 50:50) at a flow rate of 2 mL/min. To confirm the radiopharmaceutical identity, a sample of the purified material was also coinjected with a nonradiolabeled sample of BU99008. Two ^{11}C-BU99008 productions were analyzed using different HPLC conditions (Eclipse XDB-C18 column [Agilent]; 150 × 4.6 mm) (32% acetonitrile:68% ammonium formate [50 mM; pH 9]; 1.5 mL/min) to confirm that the product was chemically and radiochemically pure.

Porcine PET Studies

All animal studies were performed in accordance with the Danish Animal Experimentation Act at the Aarhus PET Centre, Denmark. Yorkshire/Danish Landrace pigs (~40 kg; $n = 3$) were kept fasting for 24 h before PET examination, with free access to water. After initial intramuscular induction of anesthesia with midazolam and ketamine, animals were intubated and put on a respirator with medical-grade air. Anesthesia was maintained with isoflurane (1.5%–2%) for the duration of the study. Catheters were surgically placed into the left femoral vein and artery of the animal for administration of radiopharmaceuticals and pharmaceutical agents and blood sampling and blood pressure recording. Throughout the study, vital signs were monitored and maintained within the normal physiologic range. Animals were placed supine in a Siemens ECAT EXACT HR tomograph, with the head immobilized in a custom-made holding device.

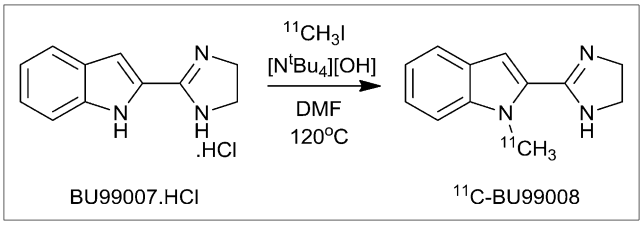

FIGURE 1. Synthesis of ^{11}C-BU99008.

In each PET experiment, 294–393 MBq of ^{11}C-BU99008 (specific activity, 51–118 GBq/μmol; injected mass of BU99008, 0.7–1.3 μg) were administered intravenously in the femoral vein as a 1-min bolus injection. Dynamic emission data were acquired in 3-dimensional mode for 90 min (26 frames; 8 × 15 s, 4 × 30 s, 2 × 1 min, 2 × 2 min, 4 × 5 min, and 6 × 10 min). Measured attenuation and scatter corrections were applied to the emission data. Data were reconstructed using the reprojection algorithm (*18*) with an axial and transaxial Hanning filter with a 0.5 cutoff frequency. The resulting images had a spatial resolution of approximately 5–7 mm in full width at half maximum (*19*). For each study, the baseline PET summed image was coregistered with a 12-parameter affine registration to the Landrace porcine brain atlas using a mutual information metric. T1-weighted MR images from 22 female Yorkshire/Landrace pigs were used to generate an atlas according to methods described previously for the Gottingen minipig (*20*). Subsequently, the transformation parameters were applied to each frame in the dynamic image of all the PET scans acquired in that study. All registrations were assessed by visual inspection, and then the regions of interest (ROIs) were applied to the dynamic images to generate regional time–activity curves.

Three studies were performed in total, each using a different pig. In studies 1 and 2, baseline scans were acquired. In study 3, a baseline scan was followed by 2 additional scans in which BU224, at doses of 0.01 and 5.00 mg/kg, was administered intravenously 30 min before injection of the radioligand.

Whole-Blood and Plasma Input Functions

Arterial blood samples (40 per scan) were collected from the femoral artery with an automated sampling system for the first 5 min and manually thereafter for the determination of whole-blood and plasma input functions. Radioactivity concentrations were measured using a γ-counter (Cobra II Auto Gamma; Packard).

Metabolite Analysis

Arterial plasma analysis of ^{11}C-BU99008 metabolism was performed for each scan as follows: arterial blood samples (5 mL) were collected at 5, 10, 20, 30, 40, 60, and 80 min after tracer injection. After centrifugation (10,000 rpm, 1 min), an equal volume of acetonitrile was added to the plasma sample. The resulting suspension was again centrifuged (10,000 rpm, 5 min), with the resulting supernatant filtered through a 0.45-mm nylon syringe filter. The deproteinized plasma samples (typically, 1.0–2.0 mL) were injected and analyzed by HPLC using an ultraviolet detector (254 nm) and a flow-through radioactivity detector. Chromatographic separation was performed using an Eclipse SB-phenyl column (150 × 4.6 mm), with a mobile phase of acetonitrile and ammonium formate (50 mM, pH 9.9; 50:50) at a flow rate of 2.0 mL/min. The fraction of unchanged radioligand was determined by the integration of the radioactivity peak corresponding to ^{11}C-BU99008 (retention time, ~5 min) and expressed as percentage of all the radioactive peaks observed.

Kinetic Analysis

Arterial plasma activity samples were fitted to a model consisting of linear interpolation before the peak and a nonnegative sum of exponentials after the peak, resulting in a continuous representation

of the total arterial plasma activity. The parent fraction was fitted using a single exponential plus a constant. The parent plasma input function was calculated as the product of the total arterial plasma curve and the fitted parent fraction curve. Whole-blood samples were linearly interpolated to generate a continuous function. A single parent fraction curve, obtained from the average across all scans in the study, was used to generate individual parent plasma concentration curves. Evident changes in the metabolism of ^{11}C-BU99008 due to the administration of BU224 were not observed; therefore, a single average parent fraction curve was selected in favor of more accurate measurements without introducing bias in the observed changes of the PET outcome measurements due to BU224 administration.

The total volume of distribution (V_T) corresponding to the ratio between tissue and plasma concentrations at equilibrium, and consisting of the sum of specific and nondisplaceable volume of distribution (V_{ND}), was derived for each ROI by curve fitting and compartmental analysis using a 1-tissue-compartment (1TC) or 2-tissue-compartment model using the parent plasma concentration as the input function. A fixed blood volume component of 5% was used in both models (*21*). Delay between the plasma parent input function and the tissue concentration was determined with a first-pass model using the first few seconds of each dynamic scan. The Akaike information criterion was used as a metric for the selection of the most parsimonious compartment model that represented the data appropriately. In addition, a time–stability analysis was performed by sequentially examining datasets with decreasing scan durations to ensure that the V_Ts obtained at 90 min were stable.

RESULTS

Radiochemistry

^{11}C-BU99008 was synthesized via the alkylation of BU99007 in *N,N*-dimethylformamide using ^{11}C-methyl iodide in the presence of tetrabutylammonium hydroxide base (Fig. 1). Under these conditions, methylation at the imidazoline nitrogen was not observed, and the reaction was found to proceed cleanly. The product was purified by semipreparative HPLC using an Eclipse SB-phenyl column (250 × 9.4 mm) and eluted with 50:50 acetonitrile:50 mM aqueous ammonium formate buffer (pH 9.9) at a flow rate of 10 mL/min. This process gave good separation of ^{11}C-BU99008 from the starting material BU99007, with retention times of 5.5 and 9.0 min, respectively (Supplemental Fig. 1; supplemental materials are available online only at http://jnm.snmjournals.org).

A typical synthesis produced 0.8–1.7 GBq of ^{11}C-BU99008 (1.2 ± 0.4 GBq at the end of synthesis), with a total synthesis time of 37 min, corresponding to a decay-corrected radiochemical yield of 22% ± 7% based on an average production of 20 GBq of ^{11}C-CH_4 from the cyclotron. Analytical HPLC (Supplemental Fig. 2) showed that the product was radiochemically pure (>99%), with specific activities of 76 ± 27 GBq/μmol at the end of synthesis.

PET

Summed PET images and corresponding time–activity curves for ^{11}C-BU99008 under baseline and blocking (5.00 mg/kg BU224) conditions are shown in Figures 2A and 2B, respectively. ^{11}C-BU99008 rapidly entered the porcine brain, reaching peak uptake levels at 10–20 min after injection (Fig. 2A). The administration of unlabeled BU224, a known I_2 ligand (*22*), was found to block the uptake of ^{11}C-BU99008 in all I_2-rich regions, leading to a near-homogeneous distribution of radioactivity throughout the brain (Fig. 2B).

Metabolite Analysis

During each PET scan, arterial plasma samples were analyzed by radio-HPLC to measure the fraction of unchanged ^{11}C-BU99008 in plasma. The first sample (5 min after tracer injection) showed a major radioactive peak eluting at 5 min, which was identified as unmetabolized ^{11}C-BU99008 by coelution with a reference sample of unlabeled BU99008. A second peak, corresponding to a more polar radiolabeled metabolite, was observed at the solvent front. The parent fraction in plasma over the course of a scan is shown in Figure 3. At 6 min after injection, the parent fraction constituted approximately 90% of the total radioactivity in plasma. This percentage decreased to approximately 40% after 20 min and approximately 20% after 40 min, when it

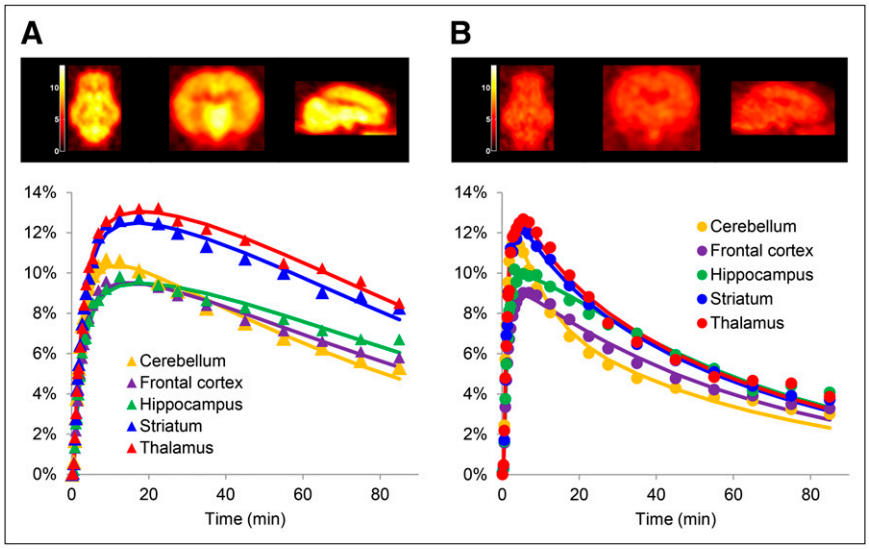

FIGURE 2. Summed PET images in porcine brain. Transverse (left), coronal (middle), and sagittal (right) images and tissue time–activity curves for ^{11}C-BU99008 for selected ROIs in porcine brain (scale bar expresses percentage injected dose per liter; lines represent 1TC model fits). (A) Baseline ^{11}C-BU99008 scan. (B) ^{11}C-BU99008 scan after administration of BU224 (5 mg/kg).

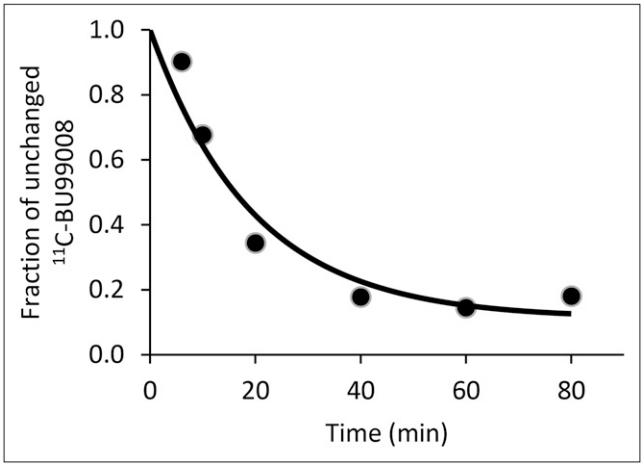

FIGURE 3. Fraction of unchanged ^{11}C-BU99008 present in plasma.

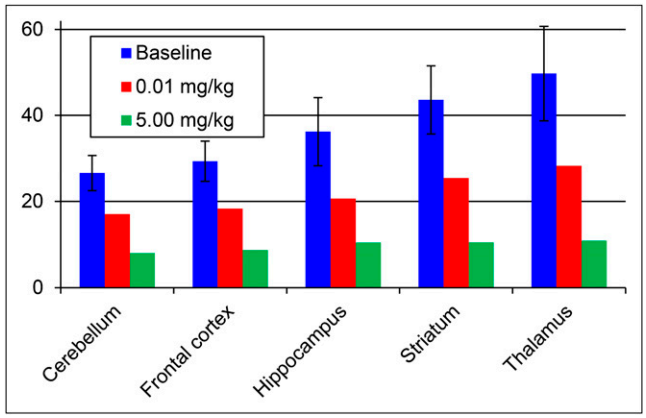

FIGURE 4. V_T estimates for selected ROIs using 1TC model for baseline ^{11}C-BU99008 scans (n = 3; mean ± SD) and scans after administration of BU224 (0.01 mg/kg, n = 1, and 5.00 mg/kg, n = 1).

plateaued until the end of the scanning session. The polar radiometabolite was assumed to be too hydrophilic to cross the blood–brain barrier. The average plasma-free fraction of BU99008 was 0.40, as determined from an equilibrium dialysis assay.

Kinetic Analysis

Time–activity curves were appropriately described by both 1TC and 2-tissue-compartment models. The Akaike information criterion metric showed that the 1TC model was the most parsimonious model and therefore was used to calculate V_T values.

Regional V_T values at baseline, and after BU224 doses of 0.01 and 5.00 mg/kg, are given in Figure 4 and Table 1. Under baseline conditions, the V_T values ranged from 26.6 (mL of plasma/cm^3 of tissue) for the cerebellum to 49.7 mL/cm^3 for the thalamus. The baseline regional V_T values can be ranked in the following order: thalamus > striatum > hippocampus > frontal cortex ≥ cerebellum and are consistent with the known distribution of I_2 binding site density throughout the brain.

The administration of a low dose of BU224 (0.01 mg/kg) caused a slight reduction in V_T values across all brain regions, with values ranging from 17.0 mL/cm^3 (cerebellum) to 28.3 mL/cm^3 (thalamus). Increasing the dose of BU224 to 5.00 mg/kg caused the V_T values to fall to relatively homogeneous levels in all brain regions, with values ranging from 8.1 mL/cm^3 (cerebellum) to 10.9 mL/cm^3 (thalamus), suggesting specificity of ^{11}C-BU99008 binding to the I_2 binding sites (Fig. 4; Table 1).

The observed decrease in the cerebellar V_T values between baseline and post-BU224 scans indicates that the cerebellum would be unsuitable for use as a reference region. To calculate V_{ND} and receptor occupancy from the BU224 blocking studies, a graphical method that obviated a reference region was used, as described previously (*23,24*). This method relies on the availability of several regions with varying levels of specific binding while assuming that the occupancy V_{ND} is constant across all regions. Under these conditions, Equation 1 can be derived, where $V_T^{Baseline}$ and $V_T^{Postdrug}$ are the regional distribution volumes for baseline and postdrug scans and Occ is the occupancy at the target site. When plotted graphically, this equation provides a simple method of calculating Occ (gradient) and V_{ND}(x-intercept).

$$V_T^{Baseline} - V_T^{Postdrug} = Occ\left(V_T^{Baseline} - V_{ND}\right), \qquad \text{Eq. 1}$$

As such, the fraction of I_2 sites occupied by BU224 (Occ) when administered at a dose of 0.01 mg/kg was calculated to be 30% and the V_{ND} equated to 3.0 mL/cm^3 (Fig. 5).

TABLE 1
V_T Estimates for Selected ROIs Using 1TC Model for Baseline ^{11}C-BU99008 Scans and Scans After Administration of BU224

V_T	Cerebellum	Frontal cortex	Hippocampus	Striatum	Thalamus
Baseline (mL/cm^3)*	26.6 ± 4.1	29.3 ± 4.7	36.2 ± 7.9	43.6 ± 7.9	49.7 ± 11.0
After BU224 administration					
0.01 mg/kg†	17.0	18.3	20.6	25.4	28.3
5.00 mg/kg†	8.1	8.8	10.5	10.6	10.9

*Data are mean ± SD; n = 3.
†n = 1.

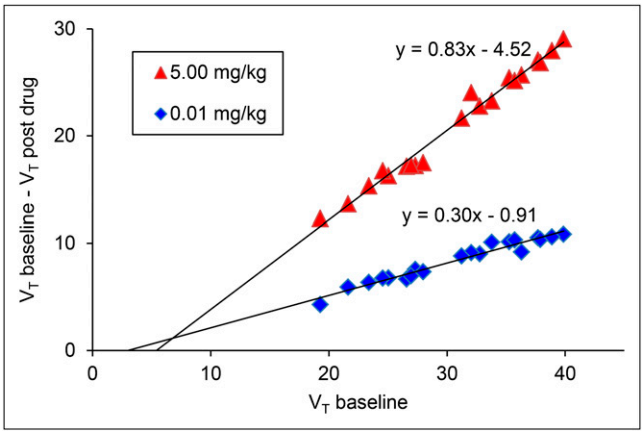

FIGURE 5. Plot of PET data obtained from 1TC model to estimate occupancy of I_2 binding sites after administrations of BU224 at 0.01 and 5.00 mg/kg.

When the BU224 dose is increased to 5.00 mg/kg, the occupancy is 83% and the V_{ND} is 5.4 mL/cm^3 (Fig. 5).

DISCUSSION

The paucity of imidazoline PET probes most likely arises from the difficulties in selecting a ligand that is readily amenable to radiolabeling while maintaining affinity and selectivity at the target. As part of our ongoing interest in the imidazoline binding sites, we sought to synthesize a new PET radioligand for I_2 sites, based around a framework that is accessible to PET radiolabeling with ^{11}C or ^{18}F. The indole analog of 2-BFI, BU99007 (Fig. 6), was chosen for this purpose because it demonstrated high affinity and selectivity for I_2 sites (*17*) while providing a means to attach the ^{11}C or ^{18}F radiolabel by substitution at the indole-nitrogen. Competition assays performed in rat whole-brain membranes revealed that the indole-*N*-substituted ligands maintain nanomolar affinity for the I_2 sites, with good selectivity over the α_2-adrenoceptors (Fig. 6) (*17*). BU99008 (R = CH_3) was identified as the choice candidate because of its high affinity for I_2 sites (1.4 nM), good selectivity (I_2/α_2 = 909), and amenability for radiolabeling via ^{11}C-methylation of BU99007 (Fig. 6).

In porcine PET studies, ^{11}C-BU99008 displayed high brain penetrance and reversible kinetics in vivo. Baseline time–activity curves showed that the binding density distribution of the radiotracer was consistent with the distribution seen in rat autoradiography studies—that is, thalamus > striatum > hippocampus > cortex > cerebellum. ^{11}C-BU99008 was found to undergo moderate metabolism in vivo, with approximately 20% of the parent compound being present at 40 min after injection.

The kinetics of ^{11}C-BU99008 are well described by a 1TC model in the porcine brain. Under baseline conditions, regional V_T values ranged from 26.6 (mL of plasma/cm^3 of tissue) for the cerebellum to 49.7 mL/cm^3 for the thalamus. The baseline regional V_T values can be ranked in the following order: thalamus > striatum > hippocampus > frontal cortex ≥ cerebellum and are consistent with the trend observed for the baseline time–activity curves.

Compound		K_i (nM)		Selectivity
		I_2	α_2	I_2/α_2
Idazoxan[a]	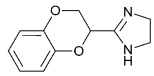	10.6 ± 1.4	55.4 ± 4.9	5.2
2-BFI[a]	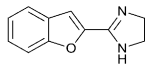	1.3 ± 0.5	3736 ± 147	2874
BU224[b]	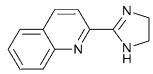	2.1 ± 0.6	12100	5762
Benazoline[c]	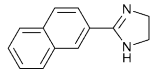	0.9 ± 0.5	15850 ± 4800	18621
FTIMD[d]	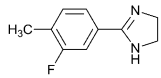	3.0	>10,000	>3333
BU99007[e]	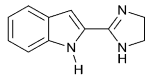	1.9 ± 0.5	4534 ± 198	2386
BU99008[e]	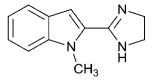	1.4 ± 0.6	1273 ± 357	909

[a]Rabbit brain against [^{3}H]idazoxan (*25*).
[b]Rat brain against [^{3}H]2-BFI (*22*).
[c]Rabbit kidney against [^{3}H]idazoxan (*26*).
[d]Rabbit kidney against [^{3}H]idazoxan (*27*).
[e]Rat brain against [^{3}H]2-BFI (*17*).

FIGURE 6. In vitro affinities of imidazoline I_2 binding site ligands.

Competition studies using the nonradiolabeled I_2 binding site ligand BU224 did not reveal a suitable reference tissue for receptor occupancy studies; hence, the graphical method was used. In these studies, ^{11}C-BU99008 binding appeared to be saturable, with I_2 binding site occupancies of 30% and 83% at BU224 doses of 0.01 and 5.00 mg/kg, respectively. The corresponding values of the V_{ND} (3.0 and 5.4 mL/cm^3 at 0.01 and 5.00 mg/kg, respectively) are close to each other, suggesting that the graphical method is indeed suitable for these calculations.

To compare the distribution of I_2 binding sites elucidated from this study with previous autoradiography studies, a correlation analysis was performed. As such, the average regional V_Ts from baseline ^{11}C-BU99008 studies can be compared with the autoradiographic distribution of I_2 binding sites determined previously using the tritiated compounds ^{3}H-2-BFI (*28*) and ^{3}H-idazoxan (*28*) (Fig. 7; Supplemental Tables 1 and 2).

A significant positive correlation ($P < 0.05$) is found between ^{11}C-BU99008 binding and the distribution of both ^{3}H-2-BFI (r^2 = 0.7548) and ^{3}H-idazoxan (r^2 = 0.7751),

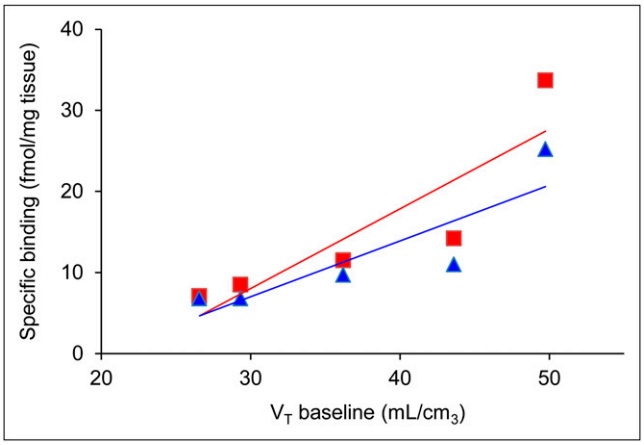

FIGURE 7. Graph showing correlation of baseline ^{11}C-BU99008 V_T values against autoradiographic distribution of I_2 ligands using ^{3}H-2-BFI (triangles) and ^{3}H-idazoxan (squares) in rat whole brain.

providing further evidence that ^{11}C-BU99008 is indeed labeling the I_2 sites in vivo in porcine brain.

CONCLUSION

The radiolabeling and initial pharmacologic investigation of ^{11}C-BU99008 as a novel PET radioligand for the I_2 binding sites has been performed. In the porcine brain, ^{11}C-BU99008 displayed reversible kinetics in vivo and a biodistribution consistent with previously reported I_2 binding site densities and localization from preclinical studies. A dose-dependent decrease in uptake of ^{11}C-BU99008 was observed after administration of pharmacologic doses of BU224. These findings suggest that ^{11}C-BU99008 may be a useful PET radioligand for the in vivo imaging of I_2 binding sites in humans.

DISCLOSURE

The costs of publication of this article were defrayed in part by the payment of page charges. Therefore, and solely to indicate this fact, this article is hereby marked "advertisement" in accordance with 18 USC section 1734. No potential conflict of interest relevant to this article was reported.

ACKNOWLEDGMENTS

We thank all the staff at the Aarhus PET centre for conducting the preclinical scans.

REFERENCES

1. Bousquet P, Feldman J, Schwartz J. Central cardiovascular effects of alpha adrenergic drugs: differences between catecholamines and imidazolines. *J Pharmacol Exp Ther.* 1984;230:232–236.
2. Eglen RM, Hudson AL, Kendall DA, et al. 'Seeing through a glass darkly': casting light on imidazoline 'I' sites. *Trends Pharmacol Sci.* 1998;19:381–390.
3. Li G, Regunathan S, Barrow CJ, Eshraghi J, Cooper R, Reis DJ. Agmatine: an endogenous clonidine-displacing substance in the brain. *Science.* 1994;263:966–969.
4. Husbands SM, Glennon RA, Gorgerat S, et al. β-Carboline binding to imidazoline receptors. *Drug Alcohol Depend.* 2001;64:203–208.
5. Finn DP, Marti O, Harbuz MS, et al. Behavioral, neuroendocrine and neurochemical effects of the imidazoline I2 receptor selective ligand BU224 in naive rats and rats exposed to the stress of the forced swim test. *Psychopharmacology (Berl).* 2003;167:195–202.
6. Sastre M, Garcia-Sevilla JA. Densities of I2-imidazoline receptors, α2-adrenoceptors and monoamine oxidase B in brains of suicide victims. *Neurochem Int.* 1997;30:63–72.
7. Sastre M, Ventayol P, Garcia-Sevilla JA. Decreased density of I2-imidazoline receptors in the postmortem brains of heroin addicts. *Neuroreport.* 1996;7:509–512.
8. Callado LF, Martin-Gomez JI, Ruiz J, Garibi JM, Meana JJ. Imidazoline I(2) receptor density increases with the malignancy of human gliomas. *J Neurol Neurosurg Psychiatry.* 2004;75:785–787.
9. Martín-Gómez JI, Ruiz J, Callado LF, et al. Increased density of I2-imidazoline receptors in human glioblastomas. *Neuroreport.* 1996;7:1393–1396.
10. Martín-Gómez JI, Ruiz J, Barrondo S, Callado LF, Meana JJ. Opposite changes in imidazoline I2 receptors and alpha2-adrenoceptors density in rat frontal cortex after induced gliosis. *Life Sci.* 2005;78:205–209.
11. García-Sevilla JA, Escriba PV, Walzer C, Bouras C, Guimon J. Imidazoline receptor proteins in brains of patients with Alzheimer's disease. *Neurosci Lett.* 1998;247:95–98.
12. Reynolds GP, Boulton RM, Pearson SJ, Hudson AL, Nutt DJ. Imidazoline binding sites in Huntington's and Parkinson's disease putamen. *Eur J Pharmacol.* 1996;301:R19–R21.
13. Dardonville C, Rozas I. Imidazoline binding sites and their ligands: an overview of the different chemical structures. *Med Res Rev.* 2004;24:639–661.
14. Roeda D, Hinnen F, Dolle F. Radiosynthesis of a 2-substituted 4,5-dihydro-^{1}H-[2-^{11}C] imidazole: the I2 imidazoline receptor ligand [^{11}C] benazoline. *J Labelled Comp Radiopharm.* 2003;46:1141–1149.
15. Kawamura K, Naganawa M, Konno F, et al. Imaging of I2-imidazoline receptors by small-animal PET using 2-(3-fluoro-[4-^{11}C]tolyl)-4,5-dihydro-^{1}H-imidazole ([^{11}C]FTIMD). *Nucl Med Biol.* 2010;37:625–635.
16. Kawamura K, Maeda J, Hatori A, et al. In vivo and in vitro imaging of I2 imidazoline receptors in the monkey brain. *Synapse.* 2011;65:452–455.
17. Tyacke RJ, Fisher A, Robinson ESJ, et al. Evaluation and initial in vitro and ex vivo characterization of the potential positron emission tomography ligand, BU99008 (2-(4,5-dihydro-1*H*-imidazol-2-yl)-1- methyl-1*H*-indole), for the imidazoline2 binding site. *Synapse.* 2012;66:542–551.
18. Kinahan PE, Rogers JG. Analytic three dimensional image reconstruction using all detected events. *IEEE Trans Nucl Sci.* 1989;36:964–968.
19. Wienhard K, Dahlbom M, Eriksson L, et al. The ECAT EXACT HR: performance of a new high resolution positron scanner. *J Comput Assist Tomogr.* 1994;18:110–118.
20. Watanabe H, Anderson F, Simonsen CZ, et al. MR-based statistical atlas of the göttingen minipig brain. *Neuroimage.* 2001;14:1089–1096.
21. Gunn RN, Gunn SR, Cunningham VJ. Positron emission tomography compartmental models. *J Cereb Blood Flow Metab.* 2001;21:635–652.
22. Hudson AL, Gough R, Tyacke R, et al. Novel selective compounds for the investigation of imidazoline receptors. *Ann N Y Acad Sci.* 1999;881:81–91.
23. Cunningham VJ, Rabiner EA, Slifstein M, Laruelle M, Gunn RN. Measuring drug occupancy in the absence of a reference region: the Lassen plot re-visited. *J Cereb Blood Flow Metab.* 2010;30:46–50.
24. Plisson C, Gunn RN, Cunningham VJ, et al. ^{11}C-GSK189254: a selective radioligand for in vivo central nervous system imaging of histamine H3 receptors by PET. *J Nucl Med.* 2009;50:2064–2072.
25. Nutt DJ, French N, Handley S, et al. Functional studies of specific imidazoline-2 receptor ligands. *Ann N Y Acad Sci.* 1995;763:125–139.
26. Pigini M, Bousquet P, Carotti A, et al. Imidazoline receptors: qualitative structure-activity relationships and discovery of tracizoline and benazoline: two ligands with high affinity and unprecedented selectivity. *Bioorg Med Chem.* 1997;5:833–841.
27. Anastassiadou M, Danoun S, Crane L, et al. Synthesis and pharmacological evaluation of imidazoline sites I1 and I2 selective ligands. *Bioorg Med Chem.* 2001;9:585–592.
28. Lione LA, Nutt DJ, Hudson AL. Characterization and localization of [^{3}H]2-(2-benzofuranyl)-2-imidazoline binding in rat brain: a selective ligand for imidazoline I2 receptors. *Eur J Pharmacol.* 1998;353:123–135.